Separated atomic ensembles: Multimode squeezed states and multipartite entangled states

Qing Xu and Xiangming Hu

Separated atomic ensembles: Multimode squeezed states and multipartite entangled states

Qing Xu[1,2] and Xiangming Hu[1]

[1] College of Physical Science and Technology, Central China Normal University, Wuhan 430079, People's Republic of China
[2] College of Physics and Electronic Information, Huanggang Normal University,
Huanggang 438000, Hubei, People's Republic of China

We show that, in analogy to light fields, effective bosonic modes of atomic ensembles in the Holstein-Primakoff representation can be prepared in multimode squeezed states, and multipartite continuous variable cluster and Greenberger-Horne-Zeilinger (GHZ) entangled states. Our scheme uses a cascade of optical cavities, in each of which one atomic ensemble is placed. Through Raman transitions between stable atomic ground states, the atomic ensembles are in the interactions with the cavity and laser fields. Because of the long-lived ground states, the atomic ensembles act as quantum network nodes, whose cluster entangled states are applicable in the one-way quantum computer, and whose GHZ entangled states have potential for quantum communiations.

I. INTRODUCTION

Squeezed state is one of the key concepts in quantum optics and finds its wide applications in the high-precision measurement [1]. Squeezing of an optical field is defined as a reduction of the quantum fluctuations in one quadrature below the standard quantum limit at the expense of the enhanced fluctuations in the conjugate quadrature [2]. Squeezing can occur for quadratures of single modes, two or more modes. The two- or multi-mode squeezing takes place when a collective operator has its noise below the standard quantum limit. This is exclusive for multiple fields because it happens even when no individual field is squeezed.

The extreme importance of two- or multi-mode squeezing is the close relation to the bipartite or multipartite continuous variable (CV) entanglement [3–8], which is an indispensable resource in quantum information and quantum communication networks [9]. Two important classes of multipartite CV entangled states are Greenberger-Horne-Zeilinger (GHZ) state [10] and cluster state [11]. The multipartite CV GHZ entangled state is a multimode (N-partite) momentum (position) eigenstate with total momentum $\sum_{l=1}^{N} p_l = 0$ (total position $\sum_{l=1}^{N} x_l = 0$) and relative positions $x_j - x_k = 0$ (relative momenta $p_j - p_k = 0$), $j = k = 1, 2, \cdots, N$, $j \neq k$. The GHZ entangled state is used for quantum teleportation [12–17], dense coding [17–20], and quantum secret sharing [21–23]. Su et al. [24] have prepared the quadripartite GHZ entangled states experimentally. The tripartite and quadripartite GHZ entanglements have been studied in the parametric interactions [25–28] and in the semiconductor [29]. On the other hand, the cluster entangled states are such that in the limit of infinite squeezing, the states become zero eigenstates of a set of quadrature combinations, $p_i - \sum_{j \in N_i} x_j \to 0$, $\forall i \in N$. In terms of a graph state, every mode $i \in N$ represents a node and the modes $j \in N_i$ are the nearest neighbors of mode i. There is an exception that a tripartite linear cluster state is up to local unitary operation equivalent to a tripartite GHZ state [30, 31]. The cluster state is applied to one-way quantum computer [32–35]. The multipartite optical cluster entanglement has been studied extensively. Su et al. [24] and Yukawa et al. [36] have prepared the quadripartite cluster entangled states experimentally.

Parallel to the squeezing and entanglement of light fields, the squeezing and entanglement of atomic ensembles has received great attention as well [37–44]. In the Holstein-Primakoff representation [45] atomic ensembles are treated as effective bosonic modes. Similarly, the atomic squeezing can occur for the quadratures of single, two, or more ensembles, and the two-mode or multimode squeezing is closely related to the bipartite or multipartite CV entanglement. The squeezed atomic ensembles are not only used in high-precision spectroscopy [38] and atomic clock, but also serve as quantum memories in the quantum networks [46–48]. Kuzmich et al. [40] proposed a scheme for spin squeezing in an ensemble of atoms by transferring quantum state from nonclassical light to atoms, and then Hald et al. [41] performed the experimental observation by using cold atoms. Choi et al. [42] demonstrated mapping of an entangled state of photons into and out of an atomic ensemble. Julsgaard et al. [43] verified a quantum memory for CV entanglement. Kuzmich et al. [44] observed the spin squeezing by monitoring continuous quantum nondemolition of a collective atomic spin with an off-resonant laser beam. Duan et al. [49] proposed that bipartite entanglement can be generated between distant free space atomic ensembles by using only coherent light pulse, and then Julsgaard et al. [43] gave the experimental verification. Parkins et al. [50] proposed a scheme for the unconditional preparation of two-mode squeezing of separated atomic ensembles. Their scheme is based on the light-atom Raman interactions in one or two optical cavities. To our knowledge, however, so far the experimental progress in atomic squeezing and CV entanglement has mainly confined to the two-mode case.

Here we generalize the scheme of Parkins et al. [50] to arbitrarily many separated atomic ensembles and show that it is possible to prepare multimode squeezed states and multipartite cluster and GHZ entangled states. Our scheme uses a cascade of cavities, in each of which one
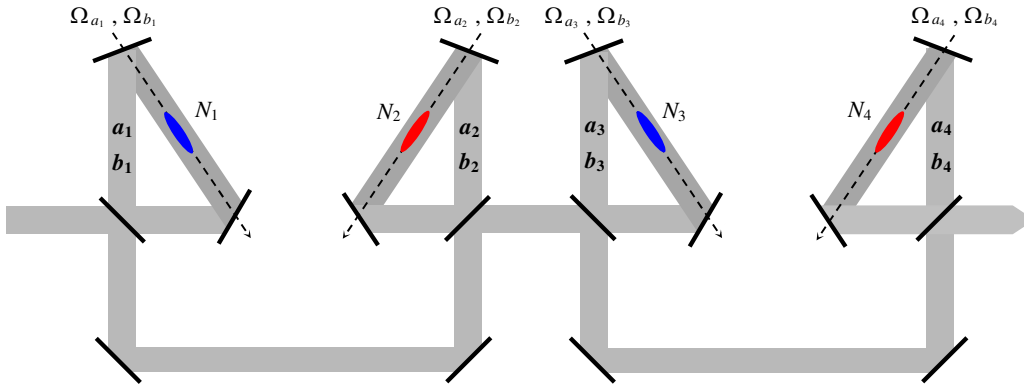
FIG. 1: (Color online) A scalable scheme for the generation of multimode squeezed states and multipartite cluster and GHZ entangled states of atomic ensembles in a cascade of optical cavities. The atomic ensembles are divided in two groups, one of which is for m ensembles on the lower right arms with the numbers of atoms $N_{1,3,\cdots,2m-1}$, and the other is for n ensembles on the lower left arms with the numbers of atoms $N_{2,4,6,\cdots,2n}$.

atomic ensemble is placed. It is shown that multimode squeezed states and multipartite CV entanglement of cluster and GHZ types are achievable. The advantage of the present scheme lies in the following four aspects. First, the multipartite entanglement is unconditionally prepared as proposed for the two-mode case [50], but not probabilistically, as proposed in Ref. [51]. Second, the multipartite entanglement is generated without the preparation of light entanglement, as in the quantum state transfer scheme from light to atoms [42, 43]. This is based on the interaction of the atoms with the cavity and laser fields. Thirdly, the present scheme avoids selective interactions as required in Ref. [52], where quadripartite case was considered and the selective interaction was used. In that scheme, however, particularly chosen sequences for the atom-field interactions, interaction times, and different phases of the driving fields were required. For the more parties, such operations become so complicated and challenging. Instead, the present scheme is suitable for arbitrarily many parties. Fourthly, this scheme is robust against spontaneous emission because the interactions of the atoms with cavity and laser fields occur between long lived ground states.

II. MODEL AND EQUATION

In Fig. 1 we depict a cascade of cavities, in each of which one ensemble of atoms is placed. Each atomic ensemble has two stable ground states (denoted by $|1\rangle$ and $|2\rangle$) and two excited states (labeled as $|3\rangle$ and $|4\rangle$), as shown in Fig. 2. The quantum transitions due to the cavity and laser fields are in the Raman configurations. The atomic ensembles under consideration are arranged into two families, i.e., one is for those that are placed on the lower right arms and labeled by the numbers N_j of atoms with odd subscripts ($j = 1, 3, 5, \cdots, 2m - 1$), and the other is for those that are placed on the lower left arms with even number subscripts ($j = 2, 4, 6, \cdots, 2n$).
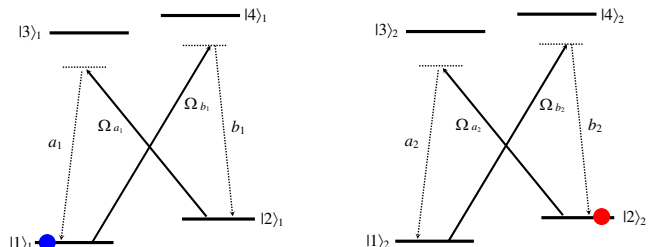

FIG. 2: (Color online) Atomic energy-level structures and quantum transitions due to the cavity fields ($a_{1,2}$ and $b_{1,2}$) and the driving fields ($\Omega_{a_{1,2}}$ and $\Omega_{b_{1,2}}$). The left part is for the atomic ensembles on the first lower-right arm in Fig. 1 and the right one is for the atomic ensemble on the first lower-left arm.

The atomic ensembles on the lower right arms are initially prepared in the state $|1\rangle$, while those on the lower left are initially prepared in the state $|2\rangle$. The light is assumed to circulate unidirectionally in the cavity. The laser fields of angular frequencies ω_{a_j} and ω_{b_j} interact with the atoms via Rabi frequencies Ω_{a_j} and Ω_{b_j}, respectively. The cavity modes a_j and b_j of angular frequencies ν_{a_j} and ν_{b_j} are coupled to the atoms with the strengths g_{a_j} and g_{b_j}, respectively. We derive the master equation for the cascade of atomic ensembles through three steps as follows.

(1) *Hamiltonian for the interaction of atomic ensembles with the cavity and laser fields.* In the dipole approximation and in an appropriate frame rotating at atomic resonance transition frequencies, the Hamiltonian of the system is written as

$$H = H_0 + H_1 + H_2, \qquad (1)$$

with

$$H_0 = \sum_j \hbar \left(\delta_{a_j} a_j^\dagger a_j + \delta_{b_j} b_j^\dagger b_j \right),$$

$$H_1 = \sum_j \hbar \left(\Omega_{a_j} \sigma_{32}^{(j)} e^{-\mathrm{i}\Delta_{a_j} t} + \Omega_{b_j} \sigma_{41}^{(j)} e^{-\mathrm{i}\Delta_{b_j} t} \right) + \mathrm{H.c.},$$

$$H_2 = \sum_j \hbar \left(g_{a_j} a_j \sigma_{31}^{(j)} + g_{b_j} b_j \sigma_{42}^{(j)} \right) + \mathrm{H.c.}, \qquad (2)$$

where $j = 1, 3, 5, \cdots, 2m-1$ are for the atomic ensembles and the light fields associated with the lower right arms in Fig. 1, and $j = 2, 4, 6, \cdots, 2n$ involve the atomic ensembles and the fields associated with the lower left arms. H_0 is the free Hamiltonian associated with the cavity modes, H_1 presents the atom-laser-field interaction Hamiltonian, and H_2 describes the atom-cavity-field interaction Hamiltonian. $\sigma_{kl}^{(j)} = \sum_{\mu_j=1}^{N_j} |k^{\mu_j}\rangle\langle l^{\mu_j}|$ $(k, l = 1-4)$ are the dipole operators of the jth atomic ensemble for $k \neq l$ and the projection operators for $k = l$. $\Delta_{a_j} = \omega_{a_j} - \omega_{32}^{(j)}$, $\Delta_{b_j} = \omega_{b_j} - \omega_{41}^{(j)}$ are, respectively, the detunings of the laser frequencies ω_{a_j} and ω_{b_j} from the atomic resonance transition frequencies $\omega_{32}^{(j)}$ and $\omega_{41}^{(j)}$. $\delta_{a_j} = \nu_{a_j} - \omega_{31}^{(j)}$ and $\delta_{b_j} = \nu_{b_j} - \omega_{42}^{(j)}$ are the detunings of the cavity frequencies ν_{a_j} and ν_{b_j} from the atomic resonance transition frequencies $\omega_{31}^{(j)}$ and $\omega_{42}^{(j)}$, respectively. The laser frequencies are assumed to satisfy the resonance conditions $\omega_{b_j} - \omega_{a_j} = 2\omega_{0_j}$ [50], where ω_{0_j} are the difference frequencies of the two ground states of the jth atomic ensembles.

(2) *Effective Hamiltonian for the two-channel Raman processes.* For the atomic ensembles on the lower right arms, $\langle \sigma_{11}^{(j)} \rangle = N_j$ $(j = 1, 3, 5, \cdots, 2m-1)$, the collective atomic spin operators are defined as $J_j^- = \sum_{\mu_j=1}^{N_j} \sigma_{12}^{\mu_j} = (J_j^+)^\dagger$ and $J_j^z = \frac{1}{2} \sum_{\mu_j=1}^{N_j} (\sigma_{22}^{\mu_j} - \sigma_{11}^{\mu_j})$. For the atomic ensembles on the lower left arms, $\langle \sigma_{22}^{(j)} \rangle = N_j$ $(j = 2, 4, 6, \cdots, 2n)$, the collective atomic spin operators are defined as $J_j^- = \sum_{\mu_j=1}^{N_j} \sigma_{21}^{\mu_j} = (J_j^+)^\dagger$ and $J_j^z = \frac{1}{2} \sum_{\mu_j=1}^{N_j} (\sigma_{11}^{\mu_j} - \sigma_{22}^{\mu_j})$. In the Holstein-Primakoff representation [45], the collective atomic operators may be associated with harmonic oscillator annihilation and creation operators c_j and $c_j^\dagger$ $([c_j, c_j^\dagger] = 1)$ via $J_j^- = (N_j - c_j^\dagger c_j)^{1/2} c_j$ and $J_j^z = c_j^\dagger c_j - N_j/2$. When $\langle c_j^\dagger c_j \rangle \ll N_j$, the collective atomic operators are thus well approximated by

$$J_j^- \simeq \sqrt{N_j} c_j, \quad J_j^+ \simeq \sqrt{N_j} c_j^\dagger, \quad J_j^z \simeq -N_j/2. \qquad (3)$$

In the case of large detunings, the atoms interact dispersively with the cavity and laser fields, then the atomic excited states are unpopulated. For the sake of simplicity we remove the Stark shifts by tuning the cavity fields such that $\nu_{a_j} = \omega_{b_j} - \omega_{0_j} - \frac{|g_{a_j}|^2 N_j}{\Delta_{a_j}}$ and $\nu_{b_j} = \omega_{b_j} - \omega_{0_j}$ for $j = 1, 3, 5, \cdots, 2m-1$ and such that $\nu_{a_j} = \omega_{b_j} - \omega_{0_j}$ and $\nu_{b_j} = \omega_{b_j} - \omega_{0_j} - \frac{|g_{b_j}|^2 N_j}{\Delta_{b_j}}$ for $j = 2, 4, 6, \cdots, 2n$.

Then the effective Hamiltonian H_{eff} is derived as [53]

$$H_{\mathrm{eff}} = \sum_{j=1,3}^{2m-1} \hbar(\tilde{g}_{a_j} a_j^\dagger c_j + \tilde{g}_{b_j} b_j^\dagger c_j^\dagger)$$
$$+ \sum_{j=2,4}^{2n} \hbar(\tilde{g}_{a_j} a_j^\dagger c_j^\dagger + \tilde{g}_{b_j} b_j^\dagger c_j) + \mathrm{H.c.}, \qquad (4)$$

where $\tilde{g}_{a_j} = \frac{\Omega_{a_j}}{\Delta_{a_j}} g_{a_j}^* \sqrt{N_j}$ and $\tilde{g}_{b_j} = \frac{\Omega_{b_j}}{\Delta_{b_j}} g_{b_j}^* \sqrt{N_j}$, and the constant energy terms are omitted.

(3) *Master equation for the atom reduced density operator.* The Langevin equations for the cavity fields are derived as

$$\dot{a}_j = -\kappa_{a_j} a_j - \mathrm{i}\tilde{g}_{a_j} c_j + \sqrt{2\kappa_{a_j}} a_j^{\mathrm{in}},$$
$$\dot{b}_j = -\kappa_{b_j} b_j - \mathrm{i}\tilde{g}_{b_j} c_j^\dagger + \sqrt{2\kappa_{b_j}} b_j^{\mathrm{in}}, \qquad (5)$$

for $j = 1, 3, 5, \cdots, 2m-1$, and

$$\dot{a}_j = -\kappa_{a_j} a_j - \mathrm{i}\tilde{g}_{a_j} c_j^\dagger + \sqrt{2\kappa_{a_j}} a_j^{\mathrm{in}},$$
$$\dot{b}_j = -\kappa_{b_j} b_j - \mathrm{i}\tilde{g}_{b_j} c_j + \sqrt{2\kappa_{b_j}} b_j^{\mathrm{in}}, \qquad (6)$$

for $j = 2, 4, 6, \cdots, 2n$. The output of each cavity is governed by the input-output formalism $a_j^{\mathrm{in}} + a_j^{\mathrm{out}} = \sqrt{2\kappa_{a_j}} a_j$ and $b_j^{\mathrm{in}} + b_j^{\mathrm{out}} = \sqrt{2\kappa_{b_j}} b_j$. Since the output from the j-th cavity is the input of the $(j+1)$-th cavity, we have $a_j^{\mathrm{out}} = a_{j+1}^{\mathrm{in}}$ and $b_j^{\mathrm{out}} = b_{j+1}^{\mathrm{in}}$. In the case of $\kappa \gg (|\tilde{g}_{a_j}|, |\tilde{g}_{b_j}|)$, we have $a_j = a_1$ and $b_j = b_1$. In the bad cavity limit, the field variables a_1 and b_1 can be eliminated adiabatically [50, 54].

We consider the following two conditions. The first condition is

$$\frac{\Omega_{a_j} \Delta_{b_j} g_{a_j}^*}{\Omega_{b_j}^* \Delta_{a_j} g_{b_j}} = C_1 \delta_{j,\mathrm{odd}} + C_2 \delta_{j,\mathrm{even}}, \qquad (7)$$

where C_1 and C_2 are respectively the positive definite constants, $\delta_{j,\mathrm{odd}} = 1$ for $j = 1, 3, \cdots, 2m-1$, and otherwise $\delta_{j,\mathrm{odd}} = 0$, $\delta_{j,\mathrm{even}} = 1$ for $j = 2, 4, \cdots, 2n$, and otherwise $\delta_{j,\mathrm{even}} = 0$. The second condition is

$$\frac{C_1}{C_2} > \frac{G_{a_1}}{G_{a_2}} > 1, \qquad (8)$$

or equivalently $\frac{C_1}{C_2} > \frac{G_{b_2}}{G_{b_1}} > 1$, where $G_{a_1} = \left(\sum_{j=1,3}^{2m-1} |\tilde{g}_{a_j}|^2 \right)^{1/2}$, $G_{a_2} = \left(\sum_{j=2,4}^{2n} |\tilde{g}_{a_j}|^2 \right)^{1/2}$, $G_{b_j} = G_{a_j}(a \to b)$. The above two conditions are met by tuning the laser fields and/or manipulating the numbers of atoms. It is convenient to introduce the collective modes $\tilde{c}_{1,2}$

$$\tilde{c}_1 = \sum_{j=1,3}^{2m-1} \frac{\tilde{g}_{a_j}}{G_{a_1}} c_j, \quad \tilde{c}_2 = \sum_{j=2,4}^{2n} \frac{\tilde{g}_{a_j}^*}{G_{a_2}} c_j. \qquad (9)$$

From now on, for convenience of description, we call c_j an odd (even) mode when j is an odd (even) number. By such definitions, we see that $\tilde{c}_1$ ($\tilde{c}_2$) represent a collection of the odd (even) modes. It should be noted that

although there are other $(m+n-2)$ independent modes, $\tilde{c}_3, \tilde{c}_4, \cdots, \tilde{c}_{m+n}$ (not written explicitly here), orthogonal with the $\tilde{c}_{1,2}$ modes, they are not in interactions with the cavity modes. As a particular example, for two ensembles with $r_1 = r_2 > 0$, we are reduced to the case as in Ref. [50].

Finally we derive the master equation for the reduced density operator as

$$
\begin{aligned}
\dot{\rho} &= \frac{\Gamma_1}{2}(2d_1\rho d_1^\dagger - d_1^\dagger d_1\rho - \rho d_1^\dagger d_1) \\
&\quad + \frac{\Gamma_2}{2}(2d_2\rho d_2^\dagger - d_2^\dagger d_2\rho - \rho d_2^\dagger d_2),
\end{aligned} \tag{10}
$$

where d_1 and d_2 are expressed as

$$
\begin{aligned}
d_1 &= \tilde{c}_1 \cosh r_1 + \tilde{c}_2^\dagger \sinh r_1, \\
d_2 &= \tilde{c}_2 \cosh r_2 + \tilde{c}_1^\dagger \sinh r_2,
\end{aligned} \tag{11}
$$

with the parameters r_1 and r_2

$$
r_1 = \operatorname{arctanh}\left(\frac{G_{a_2}}{G_{a_1}}\right), \quad r_2 = \operatorname{arctanh}\left(\frac{G_{b_1}}{G_{b_2}}\right), \tag{12}
$$

and the decay rates $\Gamma_{1,2}$ are given as $\Gamma_1 = \frac{2}{\kappa}(G_{a_1}^2 - G_{a_2}^2)$ and $\Gamma_2 = \frac{2}{\kappa}(G_{b_2}^2 - G_{b_1}^2)$.

III. QUANTUM CORRELATIONS

In this section we analyze the quantum correlations of the atomic ensembles using the master equation (10). In Sec. IIIA we first examine the properties of the multimode squeezing, then we discuss the multipartite cluster and GHZ entanglements in Sec. IIIB and in Sec. IIIC, respectively.

A. Multimode squeezed states

For simplicity, we first focus on the case of $r_1 = r_2 = r > 0$ and $\Gamma_1 = \Gamma_2$. The two collective modes $\tilde{c}_{1,2}$ have the symmetric behavior, as will be seen in the following subsection. In this case the $d_{1,2}$ modes in Eq. (11) constitute a pair of orthonormal modes, $[d_j, d_k^\dagger] = \delta_{jk}$ and $[d_j, d_k] = 0$. Therefore, the master equation (10) consists of two standard damping terms [54]. Thus the $d_{1,2}$ modes are not populated and damped into the vacuum states. Correspondingly, $\tilde{c}_{1,2}$ are both in the squeezed vacuum states at the steady state [50]. In fact, the $d_{1,2}$ modes are related to the $\tilde{c}_{1,2}$ modes through a unitary squeeze transformation, i.e.,

$$
d_{1,2} = U(r)\tilde{c}_{1,2}U^\dagger(r), \tag{13}
$$

with the squeeze operator

$$
U(r) = \exp(r\tilde{c}_1\tilde{c}_2 - r\tilde{c}_1^\dagger \tilde{c}_2^\dagger), \tag{14}
$$

where r is called the squeezing parameter. The inverse transformation is $\tilde{c}_{1,2} = U^\dagger(r)d_{1,2}U(r)$, which indicates that $\tilde{c}_{1,2}$ are both in the squeezed vacuum state at the steady state. Introducing the collective quadrature operators

$$
X_l = \frac{1}{\sqrt{2}}(\tilde{c}_l + \tilde{c}_l^\dagger), \quad P_l = \frac{1}{i\sqrt{2}}(\tilde{c}_l - \tilde{c}_l^\dagger), \tag{15}
$$

$l = 1, 2$, we can obtain their correlations [2]

$$
\begin{aligned}
\langle(\delta X_{1,2})^2\rangle &= \langle(\delta P_{1,2})^2\rangle = \frac{1}{2} + \sinh^2 r, \\
\langle\delta X_1\delta X_2\rangle &= -\langle\delta P_1\delta P_2\rangle = -\frac{1}{2}\sinh(2r).
\end{aligned} \tag{16}
$$

We further define quadrature operators

$$
X = X_1 + X_2, \quad P = P_1 + P_2, \tag{17}
$$

and obtain the quadrature fluctuations

$$
\langle(\delta X)^2\rangle = e^{-2r}, \quad \langle(\delta P)^2\rangle = e^{2r}. \tag{18}
$$

The variance $\langle(\delta X)^2\rangle$ is below the standard quantum limit 1, which reveals that the two-mode squeezing occurs in the amplitude quadrature X. In terms of the collective forms of modes $\tilde{c}_{1,2}$ in Eq. (9), the suppression of noise in X quadrature, in essence, indicates the occurrence of multimode squeezing. This is seen clearly by expanding $\tilde{c}_1$ and $\tilde{c}_2$ in Eq. (14) in terms of the individual atomic modes. After doing so, we obtain the multimode squeeze operator [55]

$$
U(\varepsilon) = \exp\left[\frac{1}{2}\sum_{j=1,3}^{2m-1}\sum_{k=2,4}^{2n}(\varepsilon_{jk}^* c_j c_k - \varepsilon_{jk} c_j^\dagger c_k^\dagger)\right], \tag{19}
$$

where $\varepsilon_{jk} = \frac{\tilde{g}_{a_j}^* \tilde{g}_{a_k}}{G_{a_1}G_{a_2}}r$ $(j = 1, 3, \cdots, 2m-1;\ k = 2, 4, \cdots, 2n)$. Applying the multimode squeeze operator $U(\varepsilon)$ to the vacuum states, we can obtain the multimode squeezed state, i.e.,

$$
|\psi\rangle = U^\dagger(\varepsilon)|0_1, 0_3, \cdots, 0_{2m-1}, 0_2, 0_4, \cdots, 0_{2n}\rangle. \tag{20}
$$

In addition, the case for $r_1 \neq r_2$ becomes complicated and we no longer give the further description. However, it can be analyzed in the same way as below for the discussion of the multipartite entanglement.

B. Multipartite cluster entanglement

Now we turn to discussing the possibilities of obtaining the cluster entangled states, as represented by two-colorable graph states in Fig. 3, where each vertex stands for one atomic mode, and each edge for the interaction between an odd atomic mode and an even one. We consider m odd modes and n even modes. When $m = 1$, $n \geqslant 2$ (or $n = 1$, $m \geqslant 2$), the networks are in the star-like configurations as shown in (i, iii and vi) of Fig. 3. For $(m, n) \geqslant 2$, we have at least one quadrilateral configuration, as shown in ii, iv, v, vii-ix) of Fig. 3. It should
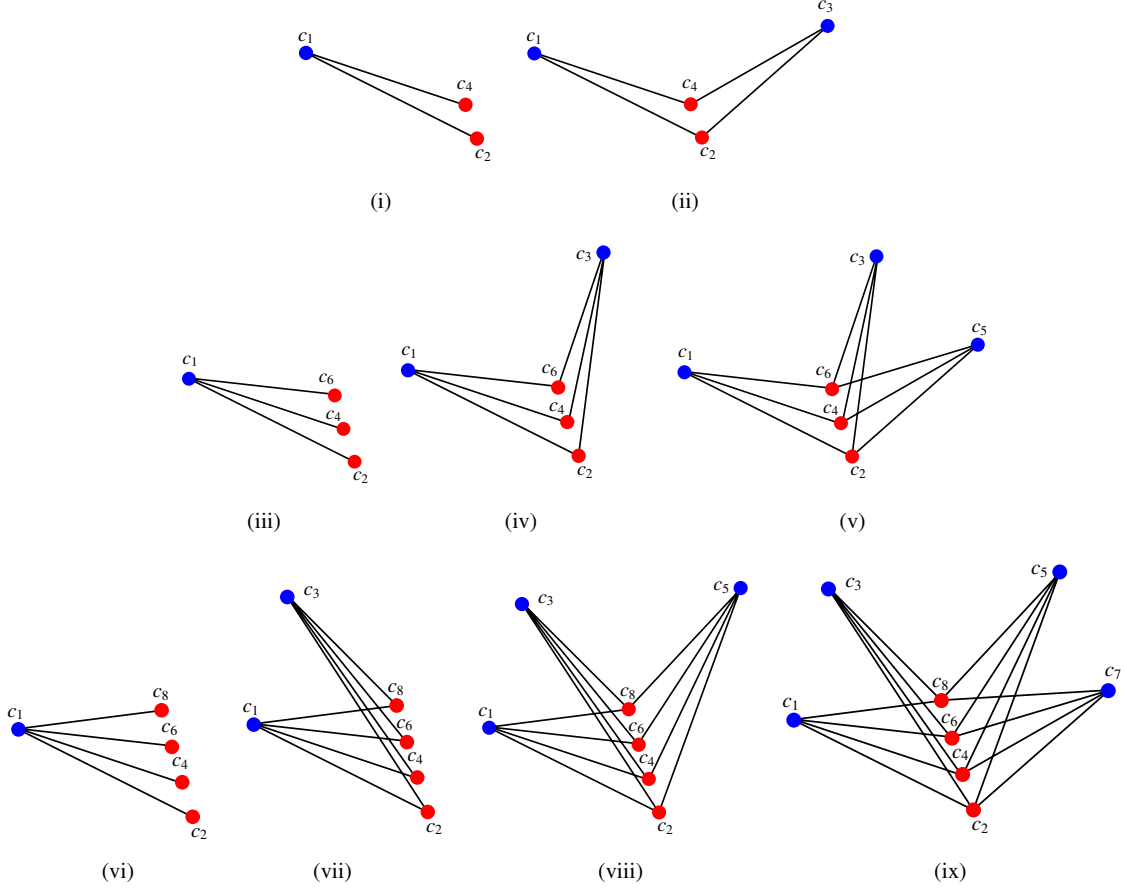
FIG. 3: (Color online) Graphical representation for the cluster states, where each vertex stands for one mode, and each edge for the interaction between the odd and even modes. It should be noted that the tripartite cluster state in (i) is equivalent to the tripartite GHZ state [30, 31].

be noted that the tripartite cluster configuration as in (i) is equivalent to the tripartite GHZ state [30, 31].

As a general case we include the cases of both $r_1 = r_2$ and $r_1 \neq r_2$. To do so, we define the parameter ratio

$$q = \frac{r_2}{r_1}. \tag{21}$$

$q = 1$ corresponds to the case $r_1 = r_2$ and $q \neq 1$ to the case of $r_1 \neq r_2$. To explore the quantum correlations for the above two cases, we employ the generalized P representation [57, 58] to transform the master equation into the Langevin equations for the c numbers. We choose a definite operator order: $c_2^\dagger$, $c_1^\dagger$, c_1, c_2, and use the correspondences of the operators to the c-numbers $\alpha_2^* \leftrightarrow \tilde{c}_2^\dagger$, $\alpha_1^* \leftrightarrow \tilde{c}_1^\dagger$, $\alpha_1 \leftrightarrow \tilde{c}_1$, $\alpha_2 \leftrightarrow \tilde{c}_2$. Substituting $d_{1,2}$ into the master equation (10), we derive the Langevin equations as

$$\frac{d\alpha_1}{dt} = \tilde{\lambda}_1 \alpha_1 - \chi \alpha_2^* + F_{\alpha_1},$$
$$\frac{d\alpha_2}{dt} = \tilde{\lambda}_2 \alpha_2 + \chi \alpha_1^* + F_{\alpha_2}, \tag{22}$$

where we have defined $\tilde{\lambda}_j = \lambda_j - \gamma_j$ and $\chi = \chi_1 - \chi_2$, with $\lambda_1 = \frac{1}{2}\Gamma_2 \sinh^2 r_2$, $\lambda_2 = \frac{1}{2}\Gamma_1 \sinh^2 r_1$, $\gamma_j = \frac{1}{2}\Gamma_j \cosh^2 r_j$,

and $\chi_j = \frac{1}{2}\Gamma_j \sinh(2r_j)$, $j = 1, 2$. It is easily seen that at the steady-state ($t \to \infty$) the mean solutions of Eq. (22) are zero, $\langle \alpha_{1,2} \rangle = \langle \alpha_{1,2}^* \rangle = 0$. The fluctuation forces F's have zero average values $\langle F_x(t) \rangle = 0$, but follow the δ-correlations, i.e., $\langle F_x(t) F_y(t') \rangle = D_{xy} \delta(t - t')$. The nonzero diffusion coefficients are obtained as $D_{\alpha_1^* \alpha_1} = 2\lambda_1$, $D_{\alpha_2^* \alpha_2} = 2\lambda_2$, $D_{\alpha_1 \alpha_2} = -(\chi_1 + \chi_2)$, together with $D_{yx} = D_{xy}$ and $D_{x^* y^*} = D_{yx}^*$.

For convenience we define $n_1 = \langle \alpha_1^* \alpha_1 \rangle$, $n_2 = \langle \alpha_2^* \alpha_2 \rangle$ and $n_{12} = \langle \alpha_1 \alpha_2 \rangle$. The equations for these correlations are derived from Eq. (22) as

$$\frac{dn_1}{dt} = 2\tilde{\lambda}_1 n_1 - 2\chi n_{12} + D_{\alpha_1^* \alpha_1},$$
$$\frac{dn_2}{dt} = 2\tilde{\lambda}_2 n_2 + 2\chi n_{12} + D_{\alpha_2^* \alpha_2},$$
$$\frac{dn_{12}}{dt} = (\tilde{\lambda}_1 + \tilde{\lambda}_2) n_{12} + \chi(n_1 - n_2) + D_{\alpha_1 \alpha_2}, \tag{23}$$

from which we have the solutions at steady state

$$n_1 = u[2\lambda_2 \chi + 2\lambda_1(\tilde{\lambda}_2^2 + \chi^2 + \tilde{\lambda}_1 \tilde{\lambda}_2) - \tilde{\lambda}_2 \chi(\chi_1 + \chi_2)],$$
$$n_2 = u[2\lambda_1 \chi + 2\lambda_2(\tilde{\lambda}_1^2 + \chi^2 + \tilde{\lambda}_1 \tilde{\lambda}_2) + \tilde{\lambda}_1 \chi(\chi_1 + \chi_2)],$$
$$n_{12} = u[2\chi(\tilde{\lambda}_1 \lambda_2 - \lambda_1 \tilde{\lambda}_2) - \tilde{\lambda}_1 \tilde{\lambda}_2(\chi_1 + \chi_2)], \tag{24}$$
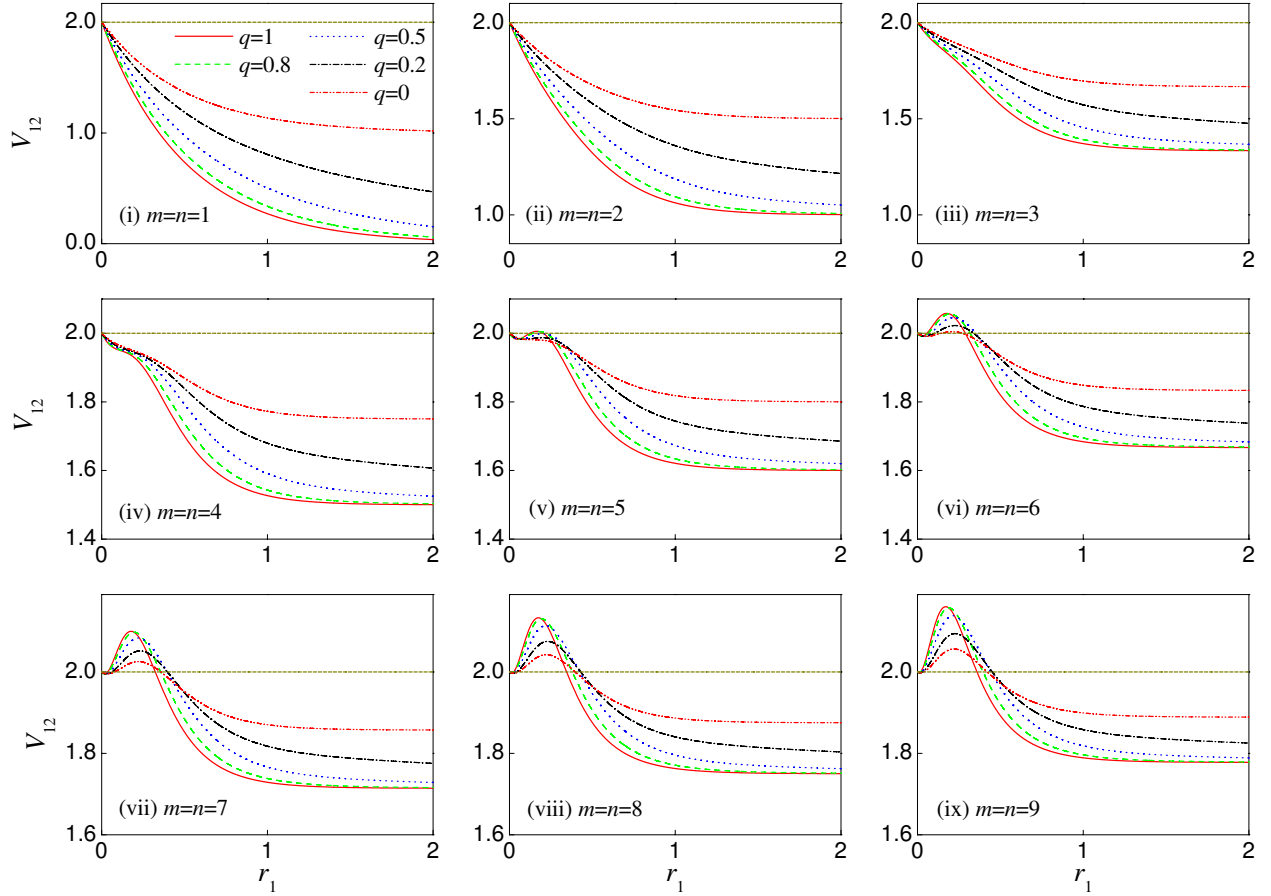
FIG. 4: (Color online) Variance V_{12} versus r_1 for $m = n = 1 - 9$ (i-ix) and $q = 1, 0.8, 0.5, 0.2, 0$.

with $u = -[2(\tilde{\lambda}_1 + \tilde{\lambda}_2)(\tilde{\lambda}_1\tilde{\lambda}_2 + \chi^2)]^{-1}$. The correlations for the quadrature operators [Eq. (15)] of the collective modes are calculated as

$$\langle(\delta X_j)^2\rangle = \langle(\delta P_j)^2\rangle = \frac{1}{2} + n_j,$$

$$\langle \delta X_1 \delta X_2 \rangle = -\langle \delta P_1 \delta P_2 \rangle = n_{12}, \quad (25)$$

with $j = 1, 2$. In particular, when $r_1 = r_2 = r$ and $\Gamma_1 = \Gamma_2$, we have $\chi = 0$, which reduces Eq. (25) to Eq. (16). In addition, from Eq. (22) we have $\langle \alpha_1 \alpha_2^* \rangle = \langle \alpha_1^* \alpha_2 \rangle = 0$. These correlations and those in Eq. (24) will be used in the following calculations of the correlations for the entanglement criteria.

According to the criteria of Loock and Furusawa [59], the multipartite CV cluster entangled states shown in Fig. 3 occurs if all of the following inequalities are satisfied simultaneously,

$$V_{jk} = \langle(\delta x_j + \delta x_k + \sum_{i=2,4;i\neq k}^{2n} \varsigma_i \delta x_i)^2\rangle$$

$$+ \langle(\delta p_j - \delta p_k + \sum_{i'=1,3;i'\neq j}^{2m-1} \varsigma_{i'} \delta p_{i'})^2\rangle < 2, \quad (26)$$

where $j = 1, 3, \cdots, 2m - 1$, and $k = 2, 4, \cdots, 2n$. The optimal factors ς's are determined by the algebraic linear

equations below

$$0 = \langle \delta x_j \delta x_l \rangle + \langle \delta x_k \delta x_l \rangle + \sum_{i=2,4;i\neq k}^{2n} \varsigma_i \langle \delta x_i \delta x_l \rangle,$$

$$0 = \langle \delta p_j \delta p_{l'} \rangle - \langle \delta p_k \delta p_{l'} \rangle + \sum_{i'=1,3;i'\neq j}^{2m-1} \varsigma_{i'} \langle \delta p_{i'} \delta p_{l'} \rangle, (27)$$

where $j, l' = 1, 3, \cdots, 2m - 1$; $l' \neq j$, and $k, l = 2, 4, \cdots, 2n$; $l \neq k$.

Here we focus on the the symmetric case, where the individual modes have the same weight in the collective modes, i.e., the collective modes take the forms $\tilde{c}_1 = \frac{1}{\sqrt{m}} \sum_{j=1,3}^{2m-1} c_j$ and $\tilde{c}_2 = \frac{1}{\sqrt{n}} \sum_{j=2,4}^{2n} c_j$. The asymmetrical case is treated in a similar way. For the symmetric case, we have $\varsigma_i = \varsigma_2$ and $\varsigma_{i'} = \varsigma_1$, and the all variances in Eq. (26) are equal, i.e., $V_{jk} = V_{12}$, for given m, n. Then we obtain the optimal factors

$$\varsigma_1 = -\frac{\sqrt{\frac{m}{n}}n_{12} + n_1}{\frac{1}{2} + (m-1)n_1},$$

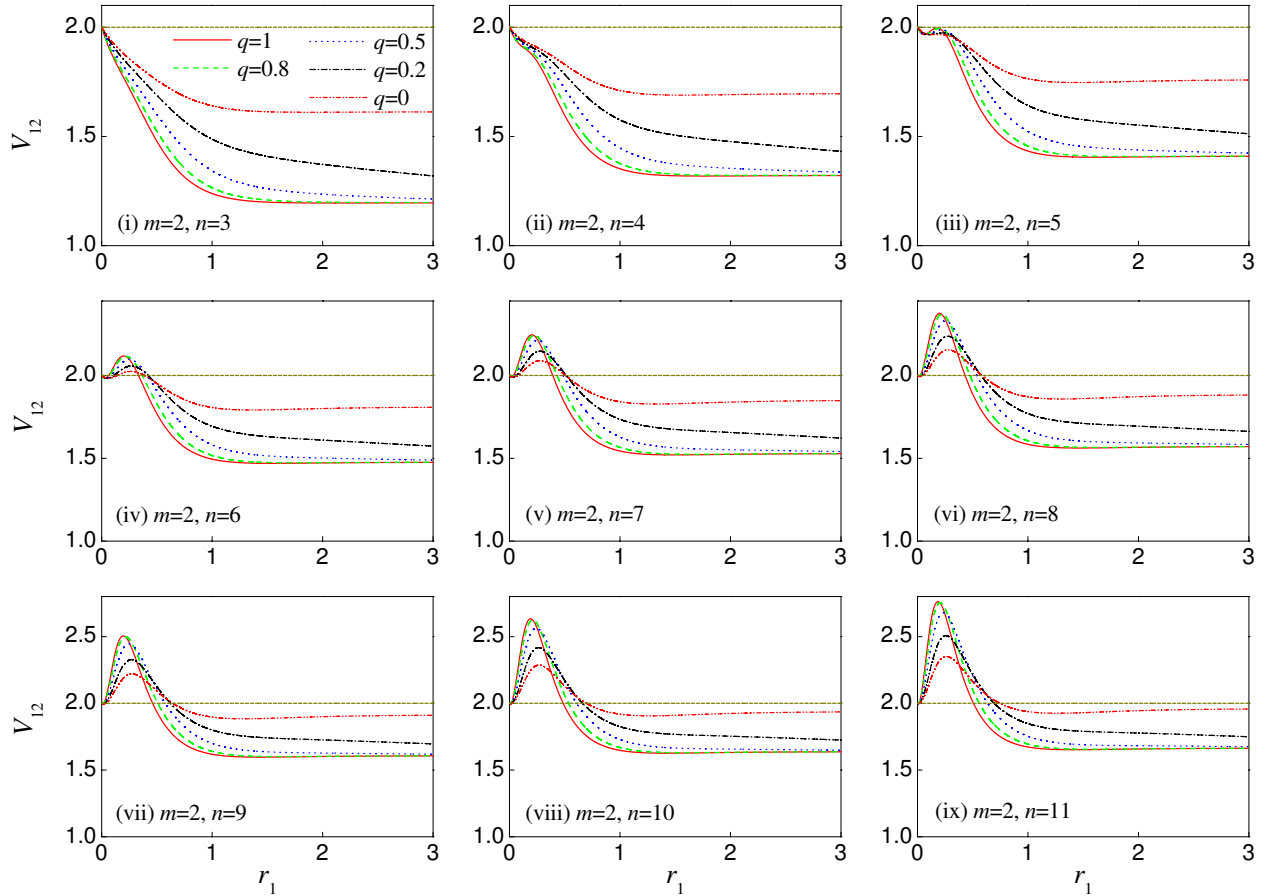$$\varsigma_2 = -\frac{\sqrt{\frac{n}{m}}n_{12} + n_2}{\frac{1}{2} + (n-1)n_2}, \quad (28)$$

FIG. 5: (Color online) Variance V_{12} versus r_1 for $m = 2$, $n = 3 - 11$ (i-ix) and $q = 1$, 0.8, 0.5, 0.2, 0.

and the variance

$$
V_{12} = \frac{2mn + n_1 n + n_2 m}{mn} + \frac{m-1}{2}\varsigma_1^2 + n_1 \tilde{\varsigma}_1^2
$$
$$
+ \frac{2n_{12}}{\sqrt{n}}\tilde{\varsigma}_1 + \frac{n-1}{2}\varsigma_2^2 + n_2 \tilde{\varsigma}_2^2 + \frac{2n_{12}}{\sqrt{m}}\tilde{\varsigma}_2, \quad (29)
$$

where $\tilde{\varsigma}_1 = \frac{1}{\sqrt{m}}[1 + (m-1)\varsigma_1]$ and $\tilde{\varsigma}_2 = \frac{1}{\sqrt{n}}[1 + (n-1)\varsigma_2]$.

So far the criteria in Eq. (26) for the multipartite entanglement is reduced to a single inequality

$$
V_{12} < 2. \quad (30)
$$

The variance V_{12} is strongly dependent on the mode numbers (m, n) and the parameters (r_1, r_2) [i.e., equivalently (r_1, q)]. The numerical results are presented in Fig. 4-6 for $q = 1$, 0.8, 0.5, 0.2, 0. We plot the variance V_{12} versus r_1 in Fig. 4 for $m = n = 1 - 9$, in Fig. 5 for $m = 2$, $n = 3 - 11$, and in Fig. 6 for $m = 1$, $n = 2 - 10$. Here we have shown only the case of $q \leqslant 1$. However, the case for $q > 1$ is similar, which is seen by noting that the plots for variance V_{12} versus r_2 are precisely the same as Fig. 4-6 when q is replaced by $1/q$ and when m is exchanged with n. We have also set $\Gamma_1 = \Gamma_2$ throughout the paper although our treatment includes the case of $\Gamma_1 \neq \Gamma_2$. For comparison we have plotted variance for the bipartite case [Fig. 4(i)]. It is seen that the entanglement criterion

is satisfied depending on the values of (m, n, r_1, q). There are three characteristic features as follows.

(1) *Cluster states for $(m, n) \geqslant 2$ occur in a broad region or even over the entire region depending on m and n.* There are two cases, one of which is for $m = n \geqslant 2$, as shown in Fig. 4, and the other is for $m \neq n$, as shown in Fig. 5. The corresponding graph state has one [Fig. 3(ii)] or even more [Fig. 3(iv-v and vii-ix)] loop configurations. For comparison we have included the $m = n = 1$ case for two parties. In these two cases, the variances exhibit the similar features. The variances are below the standard quantum limit 2 in a broad region or even over the entire region, as shown in Fig. 4 and in Fig. 5. The multipartite cluster entanglement occurs when $V_{12} < 2$. When m and n are relatively small, the inequality is easier to satisfy. As a consequence, the cluster entanglement criterion is satisfied over the whole regime, as shown in (i-iv) of Fig. 4 and in (i,ii) of Fig. 5. In contrast, when m or n is relatively large, such inequality is fulfilled only when r_1 is bigger than a certain value.

(2) *Cluster states for $m = 1$ and $n \geqslant 2$ (or for $n = 1$ and $m \geqslant 2$) exist in a narrow region.* In this case, the graph state is an open configuration and displays star-like structure, as shown in Fig. 3(i, iii and xi). The criterion $V_{12} < 2$ is met only in a limited region of r_1, i.e., the dips below the standard quantum limit, as shown in Fig.
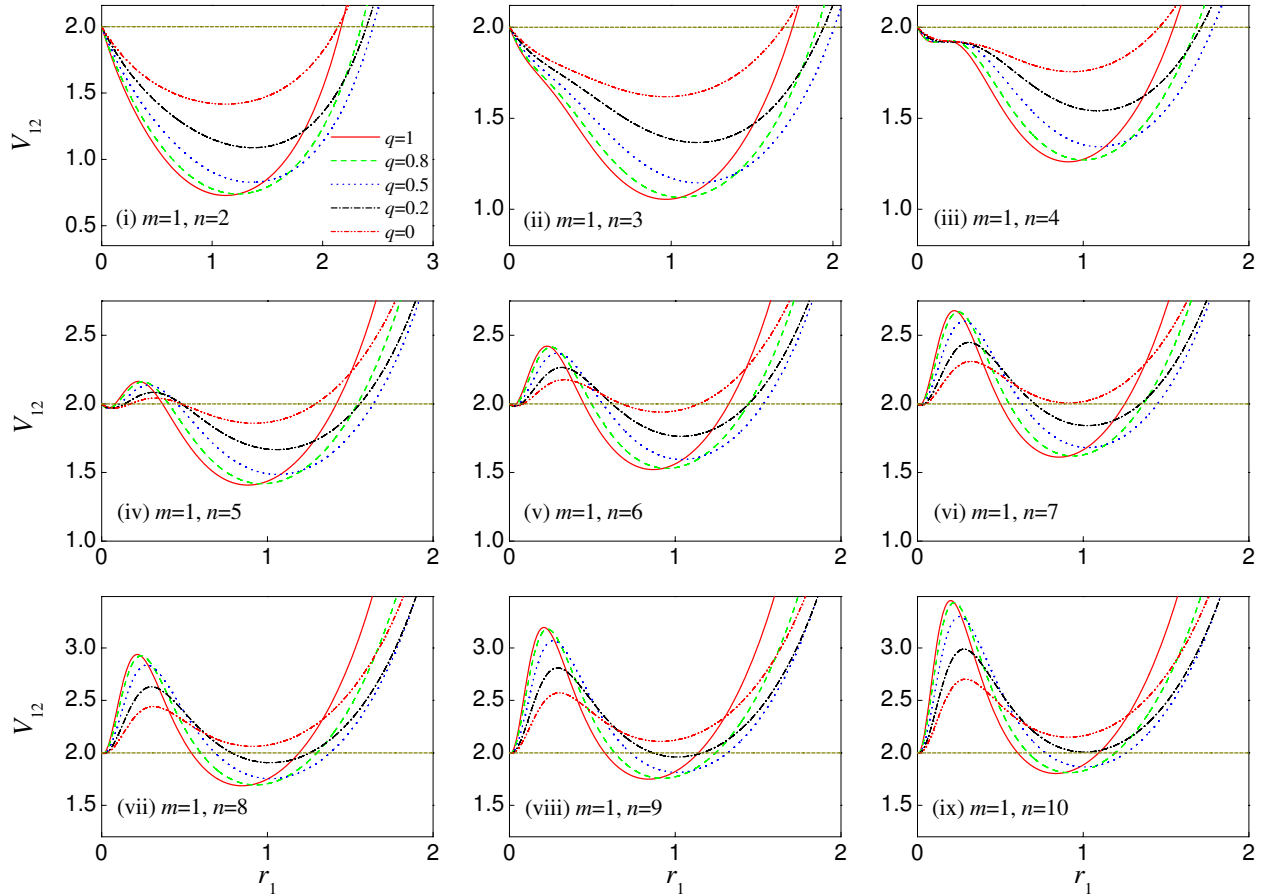
FIG. 6: (Color online) Variance V_{12} versus r_1 for $m = 1$, $n = 2 - 10$ (i-ix) and $q = 1$, 0.8, 0.5, 0.2, 0.

6. As n rises, the dips move in the upper right direction. When n is relatively small, the inequality $V_{12} < 2$ holds in a region ranging from 0 to a certain value. But when n is relatively large, the criterion $V_{12} < 2$ is satisfied only for a region of intermediate value of r_1. In addition, it should be noted that the tripartite cluster state in (ii) is equivalent to the tripartite GHZ state [30, 31].

(3) *Cluster states appear for $r_1 \neq r_2$.* We note the $m = n = 1$ case [Fig. 4(i)], which corresponds to the two parties, as discussed by Parkins *et al.* [50]. In their work, $r_1 = r_2$ is required for obtaining two-mode squeeze operator. In fact, the two-mode squeezing is existent for $r_1 \neq r_2$, including $r_1 = 0$ or $r_2 = 0$. Although this is not shown here, we have shown the quantum correlation for bipartite entanglement criterion [the solid line in Fig. 4(i)]. It shows clearly that the bipartite entanglement exists over the entire r_1 region even when $r_1 \neq r_2$. For the various multipartite cases we have relaxed the condition of $q = 1$ for entanglement. We find that even though r_1 and r_2 are remarkably different from each other (or one of them is zero), multipartite entanglement is obtainable. It is seen that the present work generalizes that of Ref. [50] in two aspects. One is for $(m, n) > 1$ and the other is for $r_1 \neq r_2$. It should also be noted that, generally, $r_1 \neq r_2$

gives rise to a negative effect on the entanglement. In comparison with the case of $r_1 = r_2$, the variance curves for $r_1 \neq r_2$ shift up, and the criterion $V_{12} < 2$ becomes relatively difficult to fulfil when m or n becomes large.

C. Multipartite GHZ entanglement

In a similar fashion, we turn to exploring the quantum correlations for the multipartite GHZ entanglement. The multipartite GHZ entanglement can be represented by graphs (as shown in Fig. 7), where each vertex stands for one atomic mode, and each edge for the interaction between arbitrarily two atomic modes. For the graphic presentation of a multipartite GHZ state, arbitrarily two of the vertices are connected with an edge. When m odd modes in Fig. 1 and n even modes are involved, we have GHZ entanglement for $m + n$ parties.

According to the criteria of Loock and Furusawa [59], the multipartite CV GHZ entangled states occurs for $m + n$ atomic ensembles if all of the following inequalities are satisfied simultaneously,
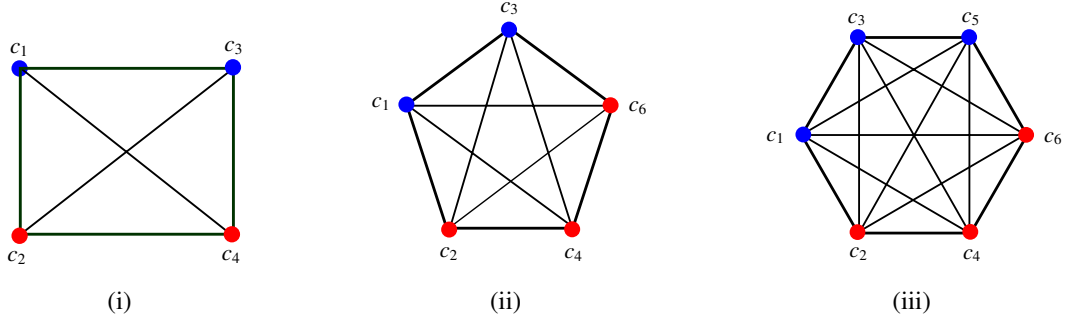
FIG. 7: (Color online) Graphical representation of CV GHZ entangled states of the effective modes $c_{1,3}$ and $c_{2,4}$ (i), $c_{1,3}$ and $c_{2,4,6}$ (ii), and $c_{1,3,5}$ and $c_{2,4,6}$ (iii), where each vertex stands for one mode, and each edge for the interaction between arbitrarily two modes.
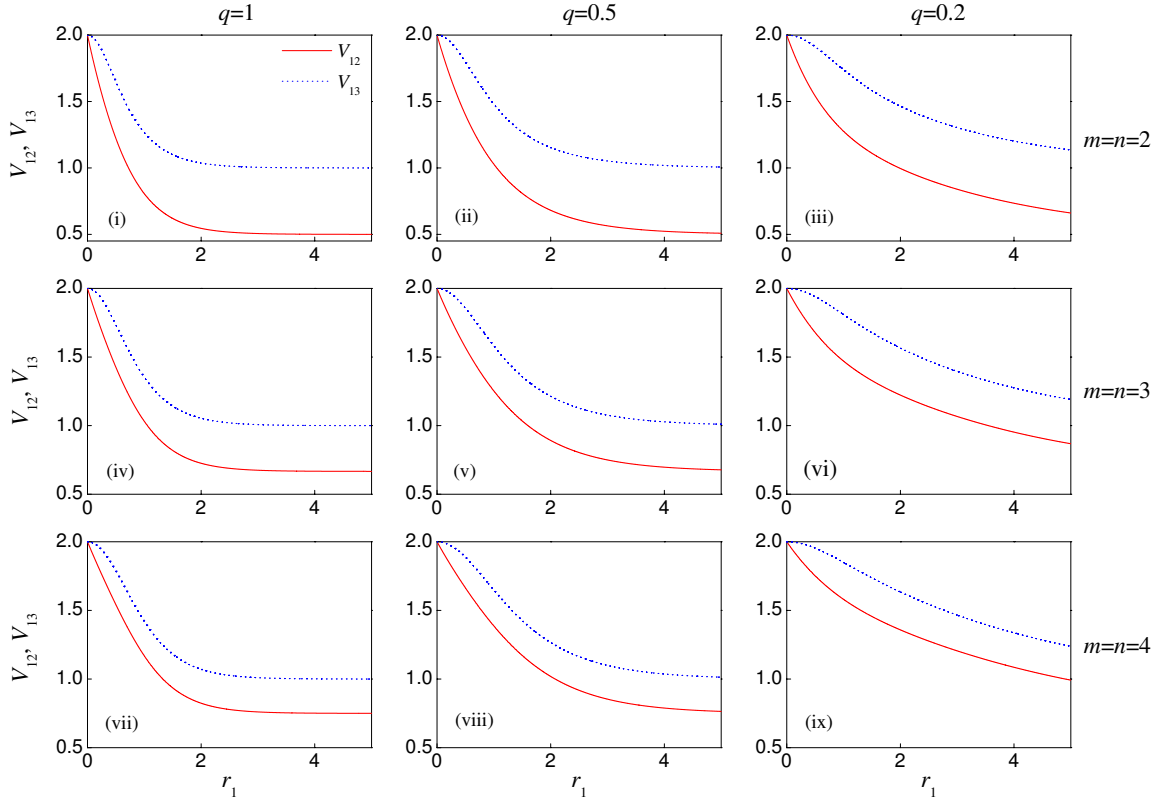

FIG. 8: (Color online) Variances V_{12} and $V_{13} = V_{24}$ versus r_1 for $m = n = 2$ (top row), 3 (middle row), 4 (bottom row) and $q = 1$ (left column), 0.5 (middle column), 0.2 (right column).

$$V_{jk} = \langle(\delta x_j + \delta x_k)^2\rangle + \langle(\delta p_j - \delta p_k + \sum_{i=1,3;i\neq j}^{2m-1} \xi_i \delta p_i + \sum_{i'=2,4;i'\neq k}^{2n} \xi_{i'} \delta p_{i'})^2\rangle < 2,$$

$$V_{jj'} = \langle(\delta x_j - \delta x_{j'})^2\rangle + \langle(\delta p_j + \delta p_{j'} + \sum_{i=1,3;i\neq j,j'}^{2m-1} \eta_i \delta p_i + \sum_{i'=2,4}^{2n} \eta_{i'} \delta p_{i'})^2\rangle < 2,$$

$$V_{kk'} = \langle(\delta x_k - \delta x_{k'})^2\rangle + \langle(\delta p_k + \delta p_{k'} + \sum_{i=1,3}^{2m-1} \zeta_i \delta p_i + \sum_{i'=2,4;i'\neq k,k'}^{2n} \zeta_{i'} \delta p_{i'})^2\rangle < 2, \tag{31}$$

where the first inequality is for $j = 1, 3, 5, \cdots, 2m-1$ and $k = 2, 4, 6, \cdots, 2n$, the second one is for $j, j' =$
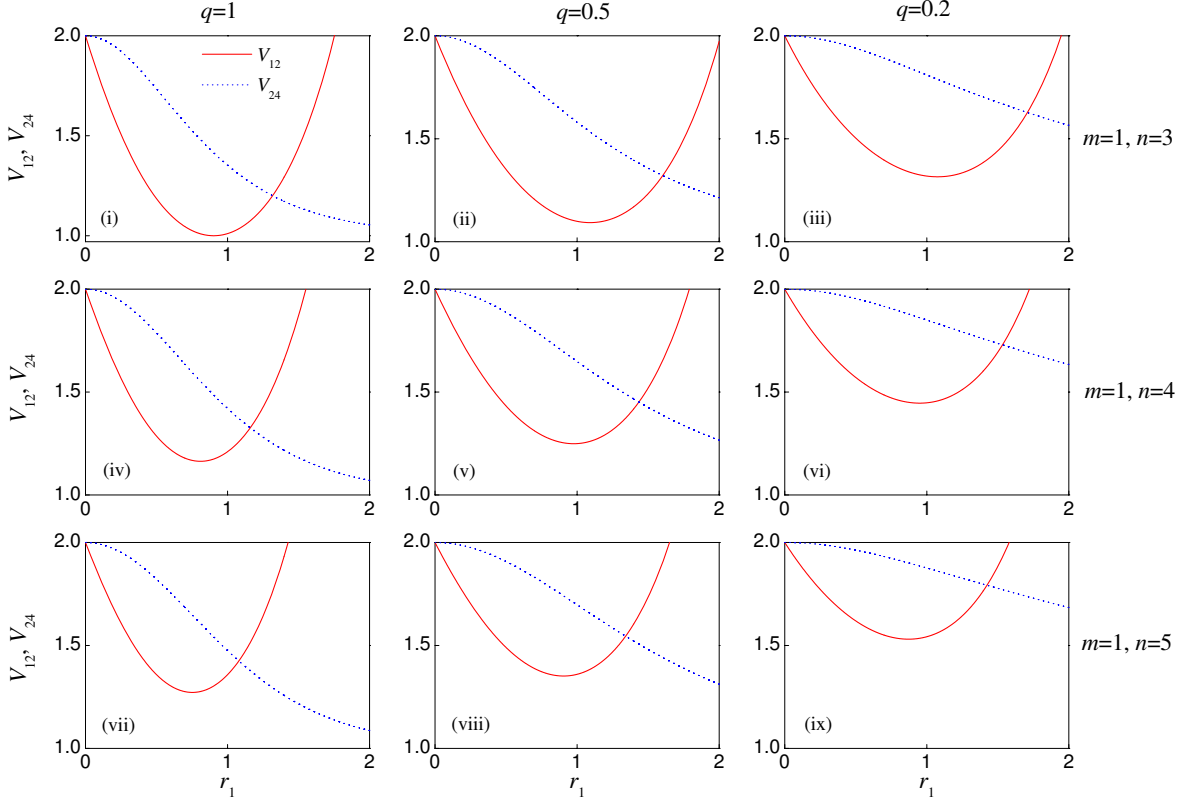
FIG. 9: (Color online) Variances V_{12} and V_{24} versus r_1 for $m = 1$, $n = 3$ (top row), 4 (middle row), 5 (bottom row) and $q = 1$ (left column), 0.5 (middle column), 0.2 (right column).

$1, 3, 5, \cdots, 2m - 1$ and $j < j'$, and the third one is for $k, k' = 2, 4, 6, \cdots, 2n$ and $k < k'$. We note that the second inequality is absent when $m = 1$ and so is the third inequality when $n = 1$. In the symmetrical case as in the above subsection, the optimal parameters in Eq. (30) become $\xi_i = \xi_1$, $\xi_{i'} = \xi_2$, $\eta_i = \eta_1$, $\eta_{i'} = \eta_2$, $\zeta_i = \zeta_1$, $\zeta_{i'} = \zeta_2$, and the variances become $V_{jk} = V_{12}$, $V_{jj'} = V_{13}$, and $V_{kk'} = V_{24}$. Then we obtain the expressions for the optimal parameters

$$\xi_1 = -u_{12}\left[\frac{n-1}{mn}(n_1 n_2 - n_{12}^2) - \frac{n_{12}}{2\sqrt{mn}} + \frac{n_1}{2m}\right],$$

$$\xi_2 = u_{12}\left[\frac{m-1}{mn}(n_1 n_2 - n_{12}^2) - \frac{n_{12}}{2\sqrt{mn}} + \frac{n_2}{2n}\right],$$

$$\eta_1 = -u_{13}\left[\frac{2}{m}n_1(n_2 + \frac{1}{2}) - \frac{2}{m}n_{12}^2\right],$$

$$\eta_2 = -u_{13}\frac{n_{12}}{\sqrt{mn}},$$

$$\zeta_1 = -u_{24}\frac{n_{12}}{\sqrt{mn}},$$

$$\zeta_2 = -u_{24}\left[\frac{2}{n}n_2(n_1 + \frac{1}{2}) - \frac{2}{n}n_{12}^2\right], \qquad (32)$$

with

$$u_{12} = \left[\frac{(m-1)(n-1)}{mn}(n_1 n_2 - n_{12}^2) + \frac{m-1}{2m}n_1 + \frac{n-1}{2n}n_2 + \frac{1}{4}\right]^{-1},$$

$$u_{13} = \left[\frac{m-2}{m}(n_1 n_2 - n_{12}^2) + \frac{m-2}{2m}n_1 + \frac{n_2}{2} + \frac{1}{4}\right]^{-1},$$

$$u_{24} = \left[\frac{n-2}{n}(n_1 n_2 - n_{12}^2) + \frac{n_1}{2}n_1 + \frac{n-2}{2n}n_2 + \frac{1}{4}\right]^{-1}, \qquad (33)$$

and the variances

$$V_{12} = 2 + \frac{m-1}{2}\xi_1^2 + \frac{n-1}{2}\xi_2^2 + \frac{n_1}{m} + \frac{n_2}{n} + \frac{2n_{12}}{\sqrt{mn}}$$
$$+ n_1\tilde{\xi}_1^2 + n_2\tilde{\xi}_2^2 + 2n_{12}\tilde{\xi}_1\tilde{\xi}_2,$$

$$V_{13} = 2 + \frac{m-2}{2}\eta_1^2 + n_1\tilde{\eta}_1^2 + \frac{n}{2}\eta_2^2 + n_2\tilde{\eta}_2^2 + 2n_{12}\tilde{\eta}_1\tilde{\eta}_2,$$

$$V_{24} = 2 + \frac{m}{2}\zeta_1^2 + n_1\tilde{\zeta}_1^2 + \frac{n-2}{2}\zeta_2^2 + n_2\tilde{\zeta}_2^2 + 2n_{12}\tilde{\zeta}_1\tilde{\zeta}_2, \qquad (34)$$
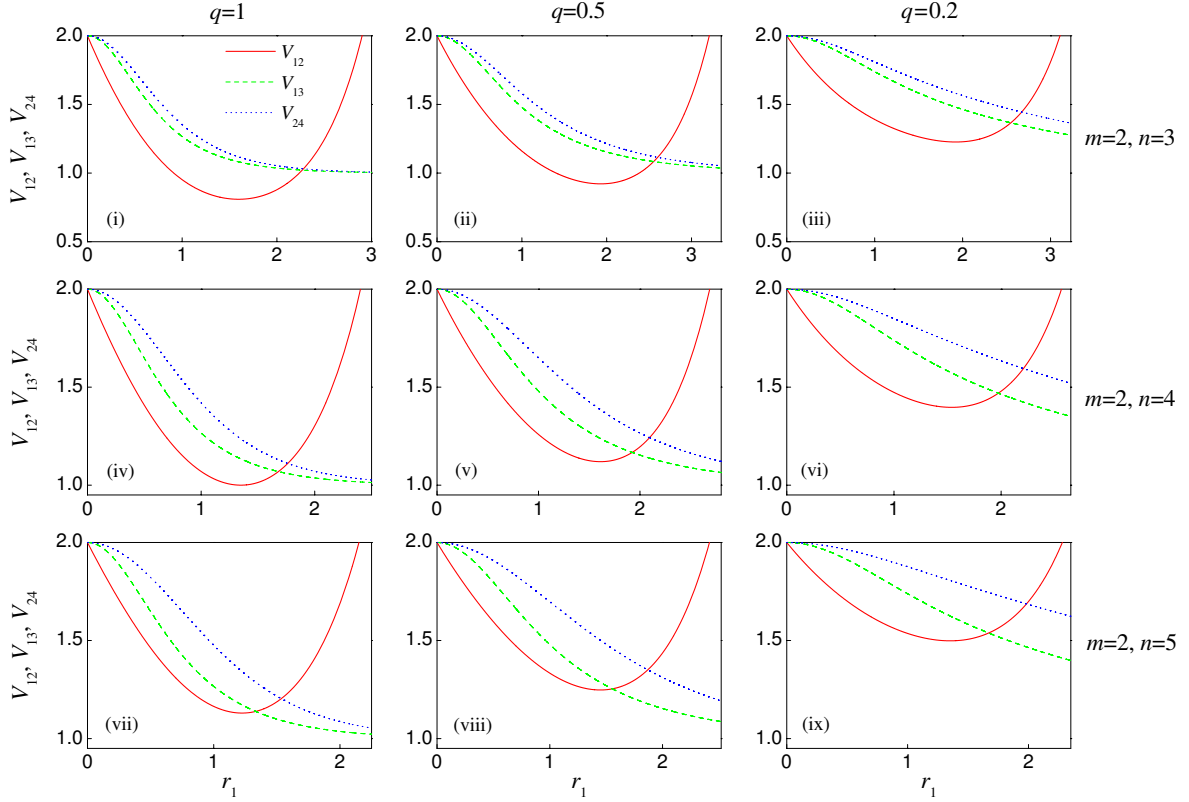
FIG. 10: (Color online) Variances V_{12}, V_{13} and V_{24} versus r_1 for $m = 2$, $n = 3$ (top row), 4 (middle row), 5 (bottom row) and $q = 1$ (left column), 0.5 (middle column), 0.2 (right column).

with

$$\tilde{\xi}_1 = \frac{1}{\sqrt{m}}[1 + (m-1)\xi_1],$$

$$\tilde{\xi}_2 = \frac{1}{\sqrt{n}}[1 + (n-1)\xi_2],$$

$$\tilde{\eta}_1 = \frac{1}{\sqrt{m}}[2 + (m-2)\eta_1],$$

$$\tilde{\eta}_2 = \sqrt{n}\eta_2,$$

$$\tilde{\zeta}_1 = \sqrt{m}\zeta_1,$$

$$\tilde{\zeta}_2 = \frac{1}{\sqrt{n}}[2 + (n-2)\zeta_2]. \quad (35)$$

Now the set of criteria in Eq. (31) for $(m, n) \geqslant 2$ are reduced to the following three inequalities

$$V_{12} < 2, \quad V_{13} < 2, \quad V_{24} < 2. \quad (36)$$

When $m = 1$ $(n = 1)$, the inequality $V_{13} < 2$ $(V_{24} < 2)$ will be absent. The variances (V_{12}, V_{13}, V_{24}) depend strongly on the mode numbers (m, n) and the parameters (r_1, r_2) [i.e., equivalently (r_1, q)]. The numerical results are presented in Figs. 8-10, where the variances are plotted as functions of r_1 for different values of (m, n, q). In all figures, the left, middle and right columns correspond to $q = 1$, 0.5, 0.2, respectively. Figure 8 shows the variances for the case of $m = n$, where we have $V_{13} = V_{24}$. The top, middle and bottom rows correspond

to $m = n = 2$, 3, 4, respectively. Note that in this case only V_{12} and V_{24} are present. Plotted in Fig. 9 are the variances for the $m = 1$ and $n = 3$ (top row), 4 (middle row), 5 (bottom row). In Fig. 10 we give the variances versus r_1 for $m = 2$ and $n = 3$ (top row), 4 (middle row), 5 (bottom row). From these figures we find that the entanglement criteria [Eq. (36)] are satisfied depending on the values of (m, n, r_1, q). Three characteristic features are presented as follows.

(1) *GHZ states for $m = n \geqslant 2$ are obtainable over the entire region.* For a given nonzero q value, the quantum correlations in Eq. (36) drop below the standard quantum limit 2 over the entire r_1 region independent of values of m and n so long as $m = n$, as shown in Fig. 8. Comparing Fig. 4 with Fig. 8, we find that the cluster states cannot appear when r_1 is relatively small, but the GHZ states always occur independent of the r_1 value.

(2) *GHZ states for $m \neq n$ are achieved in a narrow regime.* Note that such case for the cluster case happens only when $m = 1$ and $n \geqslant 2$ or when $n = 1$ and $m \geqslant 2$. For the present GHZ states, so long as $m \neq n$, the r_1 range for entanglement is limited. As shown in Fig. 9 and in Fig. 10, the inequalities in Eq. (36) are met in a narrow r_1 regime ranging from 0 to a certain value.

(3) *GHZ states happen for $r_1 \neq r_2$.* Similar to the cluster case, GHZ states can appear for the $r_1 \neq r_2$ case. The essential difference is the absence of the GHZ entanglement when $q = 0$. In addition, generally, $r_1 \neq r_2$ have

also a slight negative effect on the quantum correlations below the standard quantum limit.

IV. DISCUSSION AND CONCLUSION

So far we have presented a scalable scheme to generate multimode squeezed states and multipartite cluster and GHZ continuous variable entangled states of arbitrarily many separated atomic ensembles. The atomic ensembles are treated as the bosonic modes in the Holstein-Primakoff representation [45]. The multimode squeezing and the multipartite entanglement of atomic ensembles are equivalences of those of the optical fields. As a natural extension of two-mode case, the present scheme involves arbitrarily many separated atomic ensembles and serves as a possible example of multipartite entangled networks. The advantage is that an atomic ensemble acts as a stationary node of quantum network. Several advantages should be emphasized. First, the multimode squeezed states and the multipartite entangled states are unconditionally prepared, but not probabilistically as in Ref. [51]. Second, the multipartite entanglement is generated via the interactions of the atoms with cavity fields and laser fields, and no entanglement resource is needed, as in Refs. [42, 43]. Thirdly, the present scheme operates at steady state and avoids selective interactions as required in Ref. [52], where particularly chosen sequences for the atom-field interactions, interaction times, and different phases of the driving fields were chosen. Fourthly, this scheme is robust against spontaneous emission because the interactions of the atoms with cavity fields and laser fields are manipulated between long lived ground states.

It is interesting to compare the conditions between the present scheme and that of Parkins *et al.* [50]. In their scheme, only two modes are involved, but the numbers of the atoms in the two modes are required to satisfy two different equalities, i.e., the conditions (ii) and (iii) in Ref. [50]. In fact, when we are reduced to two modes, these two conditions are $\tilde{g}_{a_1} = \tilde{g}_{b_2}$ and $\tilde{g}_{b_1} = \tilde{g}_{a_2}$. Under such conditions, we have $r_1 = r_2$, and the two combination modes in Eq. (11) constitute a pair of orthonormal modes. This gives us a pure squeezed state. So is for the multimode cases, as shown in Sec. IIIA. Parkins *et al.* [50] also pointed out that, by their numerical simulations, for deviations of the ratio $\tilde{g}_{b_2}/\tilde{g}_{a_1}$ from unity by $10\% - 15\%$ the reduction in the Einstein-Podolsky-Rosen variance [3] is degraded (for $\tanh r = 0.8$) by only 1-2 dB. However, these two conditions become unnecessary if one does not require the pure squeezed state. As shown above in Sec. IIIB and in Sec. IIIC, both the clus-

ter and GHZ multipartite entanglements are achievable in general when $r_1 \neq r_2$. This means that we relax the conditions on the numbers of atoms in the odd and even atomic modes for the squeezing and entanglement.

As a possible experimental system, we consider these atomic ensembles consisting of $N \sim 10^6$ ^{87}Rb atoms. The ground states $|1\rangle$ and $|2\rangle$ correspond to the magnetic states $\{F = 1, m_F = \pm 1\}$, respectively. These quantum transitions are coupled via the circularly polarized cavity modes and laser fields. The degeneracy is lifted up by the external magnetic field, and the pair of Raman transitions are identified. For the realistic parameters we have the single-atom single-photon dipole coupling strength $g/(2\pi) \sim 50$ kHz [60, 61], the laser Rabi frequencies $\Omega/(2\pi) \sim 1$ MHz, the atomic excited state detunings $\Delta/(2\pi) \sim 200$ MHz. These give us Raman transition rates $\tilde{g}/(2\pi) \sim 250$ kHz. The cavity damping rate is taken as $\kappa/(2\pi) \sim 1$ MHz, which guarantees the adiabatic elimination of the cavity modes. A readout of the atomic quantum memory can be performed by coupling once more to these modes alone and adiabatically mapping their states onto the readout light fields. The rate of decoherence of the atomic quantum memory due to atomic spontaneous emission is determined by the rate of single-atom spontaneous emission, i.e., $\gamma \frac{\Omega^2}{\Delta^2} \sim 0.15$ kHz, with $\gamma/(2\pi) \sim 6$ MHz being the spontaneous decay rate of ^{87}Rb from the excited states to the ground states. Thus, the effect of spontaneous emission on the fidelity is negligibly small.

In conclusion, we have shown that the multimode squeezed states and the multipartite cluster and GHZ entangled states can occur for atomic ensembles as the correspondences of many light fields. The quantum correlations of the atomic ensembles are remarkably dependent on the atomic mode numbers (m, n) and the parameters (r_1, r_2). For $(m, n) \geqslant 2$, the cluster states are achieved in a broad $r_{1,2}$ region when (m, n) are large, or even over the entire $r_{1,2}$ region when (m, n) are relatively small. For $m = 1$ and $n \geqslant 2$ (or for $n = 1$ and $m \geqslant 2$), the cluster states exist only in a narrow $r_{1,2}$ region. It differs slightly for the GHZ states. The GHZ states are obtainable over the entire $r_{1,2}$ region so long as $m = n \geqslant 2$, but in a narrow $r_{1,2}$ region when $m \neq n$.

[1] C. M. Caves, Phys. Rev. D **23**, 1693 (1981); C. M. Caves, K. S. Thorne, R. W. P. Drever, V. D. Sandberg, and M. Zimmermann, Rev. Mod. Phys. **52**, 341 (1980).

[2] D. F. Walls and G. J. Milburn, *Quantum Optics* (Springer-Verlag, Berlin, 1995).

[3] A. Einstein, B. Podolsky, and N. Rosen, Phys. Rev. **47**, 777 (1935).

[4] E. Schrödinger, Naturwissenschaften **23**, 807 (1935).

[5] R. Horodecki, P. Horodecki, M. Horodecki, and K. Horodecki, Rev. Mod. Phys. **81**, 865 (2009).

[6] M. D. Reid, P. D. Drummond, W. P. Bowen, E. G. Cavalcanti, P. K. Lam, H. A. Bachor, U. L. Andersen, and G. Leuchs, Rev. Mod. Phys. **81**, 1727 (2009).

[7] Y. Wu, M. G. Payne, E. W. Hagley, and L. Deng, Phys. Rev. A **69**, 063803 (2004).

[8] H. Sun and X. M. Hu, J. Phys. B **44**, 205504 (2011); X. Liang, X. M. Hu, and C. He, Phys. Rev. A **85**, 032329 (2012).

[9] S. L. Braunstein and P. van Loock, Rev. Mod. Phys. **77**, 513 (2005).

[10] D. M. Greenberger, M. A. Horne, A. Shimony, and A. Zeilinger, Am. J. Phys. **58**, 1131 (1990).

[11] H.-J. Briegel and R. Raussendorf, Phys. Rev. Lett. **86**, 910 (2001).

[12] L. Vaidman, Phys. Rev. A **49**, 1473 (1994).

[13] A. Furusawa, J. L. Sørensen, S. L. Braunstein, C. A. Fuchs, H. J. Kimble, and E. S. Polzik, Science **282**, 706 (1998).

[14] A. Furusawa and N. Takei, Phys. Rep. **443**, 97 (2007)

[15] S. L. Braunstein and H. J. Kimble, Phys. Rev. Lett. **80**, 869 (1998); Nature (London) **394**, 840 (1998).

[16] H. Yonezawa, T. Aoki, and A. Furusawa, Nature (London) **431**, 430 (2004).

[17] Y. Yeo and W. K. Chua, Phys. Rev. Lett. **96**, 060502 (2006).

[18] X. Y. Li, Q. Pan, J. T. Jing, J. Zhang, C. D. Xie, and K. C. Peng, Phys. Rev. Lett. **88**, 047904 (2002).

[19] J. Zhang, C. D. Xie, and K. C. Peng, Phys. Rev. A **66**, 032318 (2002).

[20] J. T. Jing, J. Zhang, Y. Yan, F. G. Zhao, C. D. Xie, and K. C. Peng, Phys. Rev. Lett. **90**, 167903 (2003).

[21] M. Hillery, V. Bužek, and A. Berthiaume, Phys. Rev. A **59**, 1829 (1999).

[22] L. Xiao, G. L. Long, F. G. Deng, and J. W. Pan, Phys. Rev. A **69**, 052307 (2004).

[23] A. M. Lance, T. Symul, W. P. Bowen, B. C. Sanders, and P. K. Lam, Phys. Rev. Lett. **92**, 177903 (2004).

[24] X. L. Su, A. H. Tan, X. J. Jia, J. Zhang, C. D. Xie, and K. C. Peng, Phys. Rev. Lett. **98**, 070502 (2007).

[25] M. K. Olsen and A. S. Bradley, Phys. Rev. A **74**, 063809 (2006).

[26] J. Guo, H. X. Zou, Z. H. Zhai, J. X. Zhang, and J. R. Gao, Phys. Rev. A **71**, 034305 (2005).

[27] H. Y. Leng, J. F. Wang, Y. B. Yu, X. Q. Yu, P. Xu, Z. D. Xie, J. S. Zhao, and S. N. Zhu, Phys. Rev. A **79**, 032337 (2009).

[28] S. L. W. Midgley, A. S. Bradley, O. Pfister, and M. K. Olsen, Phys. Rev. A **81**, 063834 (2010).

[29] X. Y. Lü and J. Wu, Phys. Rev. A **82**, 012323 (2010).

[30] J. Zhang and S. L. Braunstein, Phys. Rev. A **73**, 032818 (2006).

[31] G. H. Low, Z. M. Shi, and Y. Yeo, Phys. Rev. A **74**, 012307 (2006).

[32] R. Raussendorf and H. J. Briege, Phys. Rev. Lett. **86**, 5188 (2001).

[33] P. Walther, K. J. Resch, T. Rudolph, E. Schenck, H. Weinfurter, V. Vedral, M. Aspelmeyer, and A. Zeilinger, Nature (London) **434**, 169 (2005).

[34] K. Chen, C. M. Li, Q. Zhang, Y. A. Chen, A. Goebel, S. Chen, A. Mair, and J. W. Pan, Phys. Rev. Lett. **99**, 120503 (2007).

[35] T. D. Ladd, F. Jelezko, R. Laflamme, Y. Nakamura, C. Monroe, J. L. O'Brien, Nature (London) **464**, 45 (2010).

[36] M. Yukawa, R. Ukai, P. van Loock, and A. Furusawa, Phys. Rev. A **78**, 012301 (2008).

[37] M. Kitagawa and M. Ueda, Phys. Rev. A **47**, 5138 (1993).

[38] D. J. Wineland, J. J. Bollinger, W. M. Itano, F. L. Moore, and D. J. Heinzen, Phys. Rev. A **46**, R6797 (1992).

[39] J. Ma, X. G. Wang, C. P. Sun, and F. Nori, Phys. Rep. **509**, 89 (2011).

[40] A. Kuzmich, K. Mølmer, and E. S. Polzik, Phys. Rev. Lett. **79**, 4782 (1997).

[41] J. Hald, J. L. Søensen, C. Schori, and E. S. Polzik, Phys. Rev. Lett. **83**, 1319 (1999).

[42] K. S. Choi, H. Deng, J. Laurat, and H. J. Kimble, Nature (London) **452**, 67 (2008).

[43] B. Julsgaard, A. Kozhekin, and E. S. Polzik, Nature (London) **413**, 400 (2001).

[44] A. Kuzmich, L. Mandel, and N. P. Bigelow, Phys. Rev. Lett. **85**, 1594 (2000).

[45] T. Holstein and H. Primakoff, Phys. Rev. **58**, 1098 (1940).

[46] R. Zhao, Y. O. Dudin, S. D. Jenkins, C. J. Campbell, D. N. Matsukevich, T. A. B. Kennedy, and A. Kuzmich, Nature Phys. **5**, 100 (2009).

[47] K. Jensen, W. Wasilewski, H. Krauter, T. Fernholz, B. M. Nielsen, M. Owari, M. B. Plenio, A. Serafini, M. M. Wolf, and E. S. Polzik, Nature Phys. **7**, 13 (2011).

[48] Y. A. Chen, S. Chen, Z. S. Yuan, B. Zhao, C. S. Chuu, J. Schmiedmayer, and J. W. Pan, Nature Phys. **4**, 103 (2008).

[49] L. M. Duan, J. I. Cirac, P. Zoller, and E. S. Polzik, Phys. Rev. Lett. **85**, 5643 (2000).

[50] A. S. Parkins, E. Solano, and J. I. Cirac, Phys. Rev. Lett. **96**, 053602 (2006).

[51] L. M. Duan , Phys. Rev. Lett. **88**, 170402 (2002).

[52] G. X. Li, S. S. Ke, and Z. Ficek, Phys. Rev. A **79**, 033827 (2009).

[53] D. F. V. James, Fortschr. Phys. **48**, 823 (2000).

[54] M. O. Scully and M. S. Zubairy, *Quantum Optics* (Cambridge University Press, Cambridge, England, 1997).

[55] C. F. Lo and R. Sollie, Phys. Rev. A **47**, 733 (1993).

[56] R. Guzmán, J. C. Retamal, E. Solano, and N. Zagury, Phys. Rev. Lett. **96**, 010502 (2006).

[57] P. D. Drummond and C. W. Gardiner, J. Phys. A **13**, 2353 (1980); P. D. Drummond and D. F. Walls, Phys. Rev. A **23**, 2563 (1981).

[58] C. W. Gardiner and P. Zoller, *Quantum Noise*, 2nd ed. (Springer-Verlag, Berlin, 2000).

[59] P. van Loock and A. Furusawa, Phys. Rev. A **67**, 052315 (2003).

[60] D. Kruse, M. Ruder, J. Benhelm, C. von Cube, C. Zimmermann, Ph. W. Courteille, Th. Elsäser, B. Nagorny, and A. Hemmerich, Phys. Rev. A **67**, 051802(R) (2003).

[61] B. Nagorny, Th. Elsäser, H. Richter, A. Hemmerich, D. Kruse, C. Zimmermann, and Ph. Courteille, Phys. Rev. A **67**, 031401(R) (2003).